

Nanoscale

Accepted Manuscript



This is an *Accepted Manuscript*, which has been through the Royal Society of Chemistry peer review process and has been accepted for publication.

Accepted Manuscripts are published online shortly after acceptance, before technical editing, formatting and proof reading. Using this free service, authors can make their results available to the community, in citable form, before we publish the edited article. We will replace this *Accepted Manuscript* with the edited and formatted *Advance Article* as soon as it is available.

You can find more information about *Accepted Manuscripts* in the [Information for Authors](#).

Please note that technical editing may introduce minor changes to the text and/or graphics, which may alter content. The journal's standard [Terms & Conditions](#) and the [Ethical guidelines](#) still apply. In no event shall the Royal Society of Chemistry be held responsible for any errors or omissions in this *Accepted Manuscript* or any consequences arising from the use of any information it contains.



Nanoscale

ARTICLE

A nitrogen-doped mesoporous carbon containing an embedded network of carbon nanotubes as a highly efficient catalyst for the oxygen reduction reaction

Received 00th January 20xx,

Jin-Cheng Li,[†] Shi-Yong Zhao,[†] Peng-Xiang Hou,^{*} Ruo-Pian Fang, Chang Liu,^{*} Ji Liang, Jian Luan, Xu-Yi Shan and Hui-Ming Cheng

Accepted 00th January 20xx

DOI: 10.1039/x0xx00000x

www.rsc.org/

A nitrogen-doped mesoporous carbon containing a network of carbon nanotubes (CNTs) was produced for use as a catalyst for the oxygen reduction reaction (ORR). SiO₂ nanoparticles were decorated with clusters of Fe atoms to act as catalyst seeds for CNT growth, after which the material was impregnated with aniline. After polymerization of the aniline, the material was pyrolysed and the SiO₂ was removed by acid treatment. The resulting carbon-based hybrid also contained some Fe from the CNT growth catalyst and was doped with N from the aniline. The Fe-N species act as active catalytic sites and the CNT network enables efficient electron transport in the material. Mesopores left by the removal of the SiO₂ template provide short transport pathways and easy access for ions. As a result, the catalyst showed not only excellent ORR activity, with 59 mV more positive onset potential and 30 mV more positive half-wave potential than a Pt/C catalyst, but also much longer durability and stronger tolerance to methanol crossover than a Pt/C catalyst.

Introduction

The electrochemical oxygen reduction reaction (ORR) is a key step that determines the performance of a variety of energy storage and conversion devices, such as fuel cells¹⁻³ and metal-air batteries^{4,5}. Pt-based catalysts have been the most efficient catalyst for ORR, but the high cost, scarcity, poor long-term stability, and poisoning effect of Pt-based catalysts significantly hinder their large-scale applications.⁶ It is therefore urgent to seek alternatives for Pt-based catalysts that have low cost, high activity and good stability.

Doped carbon materials prepared by metal-free heteroatom doping⁷⁻¹⁸ or noble-metal-free heteroatom doping¹⁹⁻²⁴ showed high electrocatalytic activity, good stability and low cost, and are therefore considered to be promising candidates for ORR catalysis. Among these, carbon-based catalysts, and nitrogen-doped carbon materials containing transition-metals (Fe and/or Co) have attracted considerable research interest due to their excellent catalytic activity.²⁵ At present, such catalysts (Me-N/C) are mainly synthesized by the pyrolysis of precursors comprised of mixtures,²⁶ composites,^{27,28} metal-organic frameworks,^{29,30} etc. of transition metals, nitrogen and carbon. However, very few Me-N/C catalysts^{21,}

³¹⁻³³ exhibit a desirable positive ORR onset potential and half wave potential, and a high reaction current compared to those of a commercial Pt/C catalyst when a similar amount of catalyst is used. To achieve excellent ORR performance, the catalyst should provide a high density of active sites, high electrical conductivity, and suitable porosity.³⁴⁻³⁶ The high electrical conductivity indicates good electron transport, micropores can supply numerous accessible active sites, and high mesoporosity facilitates efficient mass transport in the catalyst.³⁷ However, there are trade-offs between these. For example, carbon materials synthesized at high temperatures usually have good graphitic crystallinity, but the density of active sites decreases,³⁸ and high porosity may decrease the electrical conductivity.

Carbon nanotubes (CNTs) have been used in the catalytic ORR as a support material³⁹⁻⁴¹ and as a metal-free catalyst^{7,42,43}, due to its one-dimensional structure, high electrical conductivity, and good stability. It was recently reported that a non-precious-metal catalyst containing CNTs showed a good ORR performance.⁴⁴⁻⁴⁶ For example, Yao et al. reported a Fe-N-C shell closely wrapped around a core of CNTs,⁴⁴ Chung et al. prepared a nitrogen-doped CNT/nanoparticle composite electrocatalyst,⁴⁵ and Yang et al. synthesized a bamboo-like CNT-Fe₃C nanoparticle hybrid.⁴⁶ In these studies, CNTs were incorporated by either pyrolysis of pre-mixed precursors or post-synthesis dispersion, and the CNTs were used to increase the electrical conductivity. However, the porosity, density of active sites, and mass transport ability of these hybrid catalysts are not well controlled and optimized. Rational design of the structure of carbon-based catalysts is crucial for achieving excellent ORR performance.

Here, we designed and fabricated a nitrogen-doped mesoporous carbon containing a network of CNTs. The mesoporous structure

Shenyang National Laboratory for Materials Science, Institute of Metal Research, Chinese Academy of Sciences, 72 Wenhua Road, Shenyang 110016, China

E-mail: cliu@imr.ac.cn and pxhou@imr.ac.cn

[†] These authors contributed equally to this work.

Electronic Supplementary Information (ESI) available: [details of any supplementary information available should be included here]. See DOI: 10.1039/x0xx00000x

provides short pathways for efficient ion transport, and the Fe-N-C species (the very small amount of Fe is from the residue of CNT growth catalyst) provide abundant active sites, while the CNT network ensures fast electron transport^{47, 48}. As a result, this carbon-based hybrid catalyst showed a higher onset potential (59 mV) and half-wave potential (30 mV), as well as higher durability and stronger tolerance to methanol crossover than a commercial Pt/C catalyst. To the best of our knowledge, this is one of the most efficient carbon-based catalysts ever reported for ORR. Considering its low-cost and easy fabrication, the material is a promising candidate for replacing Pt-based ORR catalysts.

Experimental

Synthesis of CNT/(N-C)-X (X=700, 800 or 900)

Figure 1 is a schematic of the synthesis process of the CNT-network supported Fe-N decorated mesoporous carbon material. First, porous SiO₂ nanoparticles were immersed in a Fe(NO₃)₃ solution (Figure 1a) to obtain SiO₂ nanoparticles decorated with clusters of Fe to act as catalyst seeds for CNT growth. CNTs were then grown on the SiO₂ by the chemical vapor deposition of ethanol at 800 °C using the iron nanoparticles as catalyst. A high-density of CNTs was produced that formed a network with many connecting links between the SiO₂ particles (Figure 1b, Figure S1a). This CNT-SiO₂ hybrid was dispersed in an aqueous HCl solution, and was then mixed with an aqueous HCl solution containing aniline monomer. An ammonium peroxydisulphate (APS) solution was then added to polymerize the aniline on the CNT-SiO₂ to form a composite (CNT-SiO₂/PANI) (Figure 1c). The CNT-SiO₂/PANI composite was pyrolysed under an NH₃ atmosphere for 1 h at different temperatures of 700, 800, and 900 °C. The resulting material was washed with a HF solution and concentrated HCl to remove SiO₂ and any unstable species. Finally, mesoporous nitrogen-doped carbon interlinked by a CNT network (CNT/N-C) was obtained (Figure 1d). The samples pyrolysed at 700, 800, and 900 °C are denoted as CNT/(N-C)-700, CNT/(N-C)-800, and CNT/(N-C)-900, respectively. More details of the preparation procedure are given in supporting information.

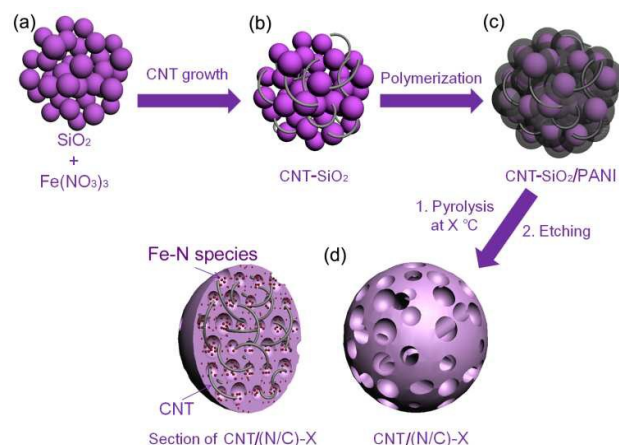


Figure 1. Schematic of the formation process of the CNT/N-C composites. (a) SiO₂ nanoparticles were immersed in an Fe(NO₃)₃ solution to load the SiO₂ with an Fe-containing catalyst precursor.

(b) CNTs were grown from the Fe catalyst on the surface of the SiO₂ nanoparticles. (c) Formation of a polyaniline matrix containing the CNT-SiO₂ hybrid by the polymerization of aniline. (d) Formation of the mesoporous nitrogen-doped carbon containing a CNT network.

Materials characterization

The morphology and structure of the catalysts were characterized using scanning electron microscopy (SEM, Nova NanoSEM 430, operated at 15 kV), X-ray diffraction (XRD, Rigaku diffractometer with CuK α radiation), X-ray photoelectron spectroscopy (XPS, Escalab 250, Al K α), Raman spectroscopy (Jobin Yvon HR800), and transmission electron microscopy (TEM, Tecnai F20, 200 kV). The specific surface area and pore structure of the samples were investigated with an automatic volumetric sorption analyzer (ASAP 2020 M) using N₂ as the adsorbate at -196 °C.

Electrode preparation and electrochemical measurements

All electrochemical measurements were performed on an electrochemical analysis station (PARSTAT 2273, CH Instruments, USA) using a standard three-electrode cell at room temperature. A Pt wire and an Ag/AgCl electrode in saturated KCl (filled with 10 wt% KNO₃ solution) served as the counter electrode and reference electrode, respectively. All potential values refer to that of a reversible hydrogen electrode (RHE). The potential difference between Ag/AgCl and RHE are based on the calibration measurements in H₂-saturated 0.1 M KOH with a Pt wire as the working and counter electrodes, and Ag/AgCl as the reference electrode.

The catalysts were ultrasonically dispersed in an ethanol solution containing 0.05 wt% Nafion to form a concentration of 2.0 mg/ml catalyst ink, then coated on the surface of a glassy carbon disk (5.0 mm diameter). The catalyst loading was 0.1 mg/cm². Cyclic voltammetric (CV) and linear sweep voltammetry (LSV) measurements were carried out in an O₂-saturated 0.1 M KOH solution. The scan rate for CV measurements was 50 mV/s and 5 mV/s for LSV measurements. The polarization curves were collected at disk rotation rates of 400, 800, 1200, 1600, 2000, and 2500 rpm. For the calculation of the number of electrons transferred (*n*), we analyzed the kinetic parameters on the basis of the Koutecký-Levich (K-L) equations.

Results and discussion

Figure 2a shows a typical scanning electron microscopy (SEM) image of the CNT/(N-C)-800 catalyst. It can be seen that CNTs are homogeneously dispersed in the porous carbon and tend to form a network. Transmission electron microscopy (TEM) observations (Figure 2b) further reveal that the CNTs are intimately rooted in the porous carbon. TEM images of catalysts prepared at different pyrolysis temperatures are shown in Figure S1. It can be seen that the carbon structure becomes more ordered as the pyrolysis temperature is increased. The pore structure of the catalysts was studied by cryo-nitrogen adsorption, and the results are given in Figure 2c, Figure S2 and Table S1. The CNT/(N-C)-800 composite shows a typical type-IV isotherm, indicating a mesoporous structure (Figure 2c). There are two distinct hysteresis loops in the medium ($P/P_0=0.45-0.6$) and high ($P/P_0=0.85-1.0$) pressure regions, which

are respectively attributed to mesopores and macropores. The right inset in Figure 2c shows that the mesopore peak widths are centered at ~ 7 nm and the average diameter of mesopores calculated by the Barrett-Joyner-Hadlenda (BJH) equation is ~ 6.6 nm. Furthermore, the rapid adsorption rise in the low pressure region indicates the presence of micropores, and the corresponding micropore distribution calculated by the density functional theory (DFT) method is plotted in the left inset of Figure 2c. It can be seen that the micropore size is centered at ~ 1.2 nm. The Barrett-Emmett-Teller (BET) surface area of the CNT/(N-C)-800 catalyst is $630 \text{ m}^2 \text{ g}^{-1}$, similar to those of the CNT/(N-C)-700 ($590 \text{ m}^2 \text{ g}^{-1}$) and CNT/(N-C)-900 ($640 \text{ m}^2 \text{ g}^{-1}$) catalysts. More details of the microstructure of the material were revealed by laser Raman spectra (Figure S3a), which shows that G-band and D-band peak shapes become slimmer with increasing pyrolysis temperature. This suggests that a higher pyrolysis temperature produces better graphitization of the mesoporous carbon, consistent with the TEM results. All the materials show X-ray diffraction (XRD) spectra with obvious (002) and (004) graphite peaks at 25° and 43° , with no other peaks observed (Figure S3b).

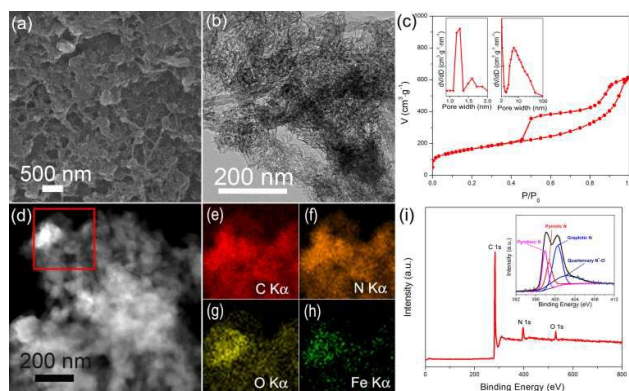


Figure 2. Typical (a) SEM and (b) TEM images of the CNT/(N-C)-800 catalyst. (c) N_2 adsorption/desorption isotherms of the CNT/(N-C)-800 catalyst (insets: (left) micro- and (right) meso-pore size distribution curves). (d) Scanning TEM (STEM) image of the CNT/(N-C)-800 catalyst and the corresponding elemental maps of (e) C, (f) N, (g) O, and (h) Fe within the square area in (d). (i) XPS spectrum of the CNT/(N-C)-800 catalyst (inset: high-resolution details of the N 1s peak).

In order to reveal the elemental composition of the CNT/(N-C)-800 catalyst, energy-dispersive X-ray spectroscopy (EDS) and X-ray photoelectron spectroscopy (XPS) characterizations were performed. Figure 2d shows a STEM image of the CNT/(N-C)-800 catalyst and the corresponding EDS element maps of C (Figure 2e), N (Figure 2f), O (Figure 2g), and Fe (Figure 2h) within the square area in Figure 2d. It is clearly shown that all these elements are uniformly distributed in the sample. An XPS survey scan (Figure 2i) confirms that the CNT/(N-C)-800 catalyst contains C (88.2 at%), N (7.4 at%), O (4.3 at%), and a small amount of Fe (< 0.1 at%, Figure S4a) from the residual Fe catalyst used for CNT growth. The inset of Figure 2i shows the corresponding high-resolution N 1s peak. The fitted peaks at 398.4, 399.1, 401.0, and 402.7 eV can be assigned to pyridinic N (20.4 at%), pyrrolic N (20.9 at%), graphitic N (35.8 at%), and quarternary N^+-O^- (22.9 at%), respectively, on the basis of their

binding energies.^{9, 49, 50} It was reported that pyridinic N and graphitic N are important active sites for ORR.^{14, 51-53} In addition, the pyridinic N and pyrrolic N can act as metal-coordination sites due to their lone-pair electrons.^{54, 55} Therefore, the high contents of pyridinic, pyrrolic, and graphitic nitrogen in the CNT/(N-C)-800 catalyst help in achieving a desirable ORR performance. We found that the content of N in the carbon-based catalyst decreases with the increasing pyrolysis temperature (Figure S4b and Table S1), and the content of nitrogen in the CNT/(N-C)-900 (3.55 at%) is only about half that in the CNT/(N-C)-800 catalyst.

The activity of the materials to electrochemically catalyze the ORR was evaluated by CV and rotating disk electrode (RDE) measurements in 0.1 M KOH. The CV curves of the CNT/(N-C)-800 in an O_2 -saturated electrolyte (Figure S5) show a distinct peak potential of 0.829 V, which is higher than that of CNT/(N-C)-700 (0.643 V) and CNT/(N-C)-900 (0.793 V) and similar to that of a Pt/C (0.833 V) catalyst. The lower potential of the CNT/(N-C)-700 can be attributed to its relatively low electrical conductivity, due to its low pyrolysis temperature and poor crystallinity as revealed by TEM, XRD and Raman. As for the CNT/(N-C)-900, despite its higher degree of graphitization, it suffers from a low N content or loss of metal-coordination sites due to its higher treatment temperature, which deteriorates its ORR activity. The ORR activity of these catalysts was further characterized by RDE measurements as shown in Figure 3a. It can be seen that the ORR activities of the catalysts are in the following order: CNT/(N-C)-800 > CNT/(N-C)-900 > CNT/(N-C)-700, consistent with the CV measurements. In particular, the CNT/(N-C)-800 catalyst exhibits outstanding ORR performance, as evidenced by an onset potential (E_{onset}) of 0.970 V, slightly higher than that of Pt/C ($E_{\text{onset}} = 0.962$ V), and a half wave potential ($E_{1/2}$) of 0.844 V, 26 mV more positive than that for Pt/C ($E_{1/2} = 0.818$ V) with the same loading density of 0.1 mg cm^{-2} as shown in Figure 3b. In addition, the limited current density (J) of the CNT/(N-C)-800 catalyst is 5.67 mA cm^{-2} , similar to that of Pt/C ($J = 5.63 \text{ mA cm}^{-2}$). When the loading amount of CNT/(N-C)-800 was increased from 0.1 to 0.5 mg cm^{-2} , improved E_{onset} and $E_{1/2}$ values of 1.021 V and 0.848 V were obtained, which are 59 mV and 30 mV, respectively, more positive than those for a Pt/C catalyst. All these results show that the CNT/(N-C)-800 catalyst has better performance than a Pt/C catalyst toward ORR in alkaline media.

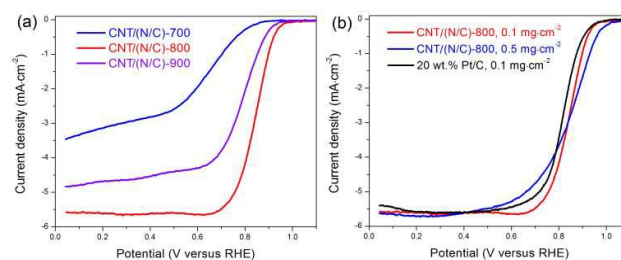


Figure 3. (a) RDE voltammograms of the CNT/(N-C)-700, CNT/(N-C)-800, and CNT/(N-C)-900 catalysts. (b) RDE voltammograms of the CNT/(N-C)-800 catalyst with low (0.1 mg cm^{-2}) and high (0.5 mg cm^{-2}) loadings and a commercial 20 wt% Pt/C catalyst. The RDE voltammograms were recorded in an O_2 -saturated 0.1 M KOH solution with a rotation rate of 1600 rpm and a scan rate of 5 mV s^{-1} .

To gain better insight into the ORR catalysis mechanism, Tafel plots of the CNT/(N-C)-800 catalyst and commercial Pt/C catalyst were derived from the RDE results (Figure S6). It can be seen that the CNT/(N-C)-800 catalyst has a Tafel slope of 66 mV/decade, much smaller than that of Pt/C (74 mV/decade), indicating that the CNT/(N-C)-800 has superior ORR kinetics and activity. A high Tafel slope means that the overpotential increases quickly with current density, leading to inferior ORR activity.⁵⁶ The lower Tafel slope of the CNT/(N-C)-800 catalyst reveals that the transfer of the first electron is probably the rate-determining step.⁵⁷ To further understand the electron transfer process of the catalysts, RDE voltammograms of the catalysts at different rotation rates (ranging from 400 to 2500 rpm) were measured, and the corresponding K-L plots at 0.4, 0.5, 0.6, and 0.7 V are given in Figures S7-S9. Using the K-L equation, J^{-1} versus $\omega^{-1/2}$ plots were obtained to estimate the electron-transfer number (n) from the slope of each line. The average value of electron-transfer number for the CNT/(N-C)-800 catalyst is 4.0, higher than those of the CNT/(N-C)-700 ($n = 3.0$) and CNT/(N-C)-900 ($n = 3.7$) catalysts. Therefore, the ORR of the CNT/(N-C)-800 catalyst follows a complete four-electron-transfer pathway compared to both the two-electron-transfer process and the four-electron-transfer process for the CNT/(N-C)-700 and CNT/(N-C)-900 catalysts. The CNT/(N-C)-800 catalyst shows a more positive onset potential and lower Tafel slope than those of commercial Pt/C catalysts. A comparison of the performance of our CNT/(N-C)-800 catalyst with that of previously reported N-doped carbon electrocatalysts^{8, 11, 58-62} is given in Figure S10. It can be seen that our CNT/(N-C)-800 catalyst shows superior ORR performance in terms of higher positive onset potential, half-wave potential, and current density. Furthermore, it is also better than most reported results of noble-metal-free catalysts (Table S2)^{21, 31, 32, 54, 63}.

We attribute the superior ORR performance of the CNT/(N-C)-800 catalyst to its unique mesoporous structure with a CNT network which simultaneously gives it a high-density of active sites, an appropriate pore structure, and good electrical conductivity. To better understand this synergistic effect, we performed comparison experiments to investigate the effect on the ORR performance of mesopores, CNTs, and residual Fe from the CNT growth. Three samples were prepared for this comparison study: first, Fe was removed from the catalyst after CNT growth and the sample is denoted no-Fe; second, the SiO₂ template was removed before the polymerization, consequently no or few mesopores exist in the sample (denoted no-MP); third, CNT growth was not performed and the sample is denoted no-CNT. The pyrolysis temperature was set to be 800 °C, and all other preparation conditions were kept unchanged. More details of the preparation procedure are given in supporting information. The contents of nitrogen in the above three samples were measured to be close to that of the CNT/(N-C)-800 catalyst (Figure S11), which suggests that the degree of nitrogen doping is mainly determined by the pyrolysis temperature. The above samples were assessed by RDE and CV measurements, and the results are shown in Figure 4a and Figure S12. From the RDE voltammograms (Figure 4a), it can be seen that the no-Fe catalyst has an obvious negative shift of $E_{1/2}$ of 20 mV, a low current density ($J = 4.84 \text{ mA cm}^{-2}$) and an electron-transfer number of 3.9 (Figure S13). The CV curves shown in Figure S11 also indicate worse ORR performance of the no-Fe catalyst than that of the CNT/(N-C)-800.

These results indicate that the residual Fe from CNT growth facilitates the formation of catalytic sites and improves the activity of the catalyst for ORR, even though the Fe content is very limited. The no-MP catalyst exhibits much poorer ORR activity than the CNT/(N-C)-800 catalyst, evidenced by a more negative E_{onset} and $E_{1/2}$, smaller J , and an incomplete four-electron-transfer pathway (Figures 4a and S14). We attribute this poor ORR performance to its lack of mesopores (Figure S15) and the low content of pyrrolic N (Figure S11). As for the no-CNT catalyst, even though it showed an E_{onset} of 0.967 V and an electron-transfer number of ~ 4.0 (Figures 4a and S16), very close to those of the CNT/(N-C)-800 catalyst, its $E_{1/2}$ and J are obviously inferior. As revealed by XPS characterization (Figure S11), the no-CNT catalyst has higher contents of pyrrolic N and Fe than those of the CNT/(N-C)-800 catalyst, which may endow it with more active sites of Fe-N species. However, the low electrical conductivity caused by the absence of conductive CNT networks and its intrinsic poor graphitization (Figure S17) impedes efficient electron transport.

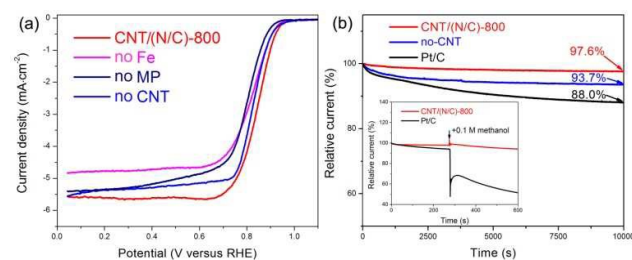


Figure 4. (a) RDE voltammograms of the CNT/(N-C)-800 catalyst and three reference catalysts for comparison. Rotation rate: 1600 rpm, scan rate: 5 mV s^{-1} . (b) Chronoamperometric responses of the CNT/(N-C)-800, no-CNT, and commercial Pt/C catalysts, 0.53 V versus RHE. Rotation rate 1600 rpm. Inset: chronoamperometric response of the CNT/(N-C)-800 and commercial Pt/C catalysts kept at 0.73 V versus RHE when 0.1M methanol was added at 280 s. Rotation rate 1600 rpm.

In addition to the high activity, we further studied the durability of the CNT/(N-C)-800 catalyst. Figure 4b shows that the current density decay of the CNT/(N-C)-800 catalyst is $\sim 2.4 \%$ after 10000 s testing, much smaller than that of commercial Pt/C ($\sim 12.0\%$), indicating excellent durability. It is interesting to point out that the CNT/(N-C)-800 catalyst also exhibits more stability than the no-CNT catalyst. Thus, the CNT framework not only leads to an increased electrical conductivity but also greatly improves the durability of the catalyst. We believe that the CNT networks and the good graphitization of the Fe-N decorated carbon play an important role in improving the stability. The tolerance of the CNT/(N-C)-800 and Pt/C catalysts toward methanol was determined by adding 0.1 M methanol into a 0.1 M KOH electrolyte during chronoamperometric measurements. As shown in the inset of Figure 4b, the current density of the CNT/(N-C)-800 remained almost unchanged while that of the Pt/C catalyst sharply decreased on the addition of methanol, suggesting that the CNT/(N-C)-800 catalyst is free from methanol crossover. These results indicate that the CNT/(N-C)-800 catalyst possesses very good structural and chemical stability, and hence has potential for use as a durable ORR catalyst.

Conclusions

In conclusion, we designed and fabricated a hybrid carbon-based catalyst that contains N-doped mesoporous carbon, a CNT network, and a small amount of Fe. The homogeneously distributed Fe-N species provide abundant active sites, the mesoporous structure enables fast and efficient mass transport, and the CNT network significantly improves the electron transport capability of the catalyst. As a result, this carbon-based catalyst shows excellent ORR activity, with a 59 mV more positive onset potential and a 30 mV more positive half-wave potential than a Pt/C catalyst. In addition, the carbon-based catalyst also shows much better durability and stronger tolerance to methanol crossover than a commercial Pt/C catalyst. Taking into account its low-cost, easy fabrication process, and excellent overall performance, the nitrogen-doped mesoporous carbon containing a network of carbon nanotubes (CNTs) is a promising candidate for use as a high-efficiency non-noble metal ORR catalyst.

Acknowledgements

This work was supported by the Ministry of Science and Technology of China (Grants 2011CB932601), National Natural Science Foundation of China (Grants 51221264 and 51272257), and Chinese Academy of Sciences (Grant KGZD-EW-T06).

Notes and references

- M. Lefèvre, E. Proietti, F. Jaouen and J.-P. Dodelet, *Science*, 2009, **324**, 71-74.
- G. Wu, K. L. More, C. M. Johnston and P. Zelenay, *Science*, 2011, **332**, 443-447.
- T. Fujigaya and N. Nakashima, *Adv. Mater.* 2013, **25**, 1666-1681.
- F. Cheng and J. Chen, *Chem. Soc. Rev.* 2012, **41**, 2172-2192.
- H.-W. Liang, X. Zhuang, S. Brüller, X. Feng and K. Müllen, *Nat. Commun.* 2014, **5**.
- C. Sealy, *Mater. Today* 2008, **11**, 65-68.
- K. Gong, F. Du, Z. Xia, M. Durstock and L. Dai, *Science*, 2009, **323**, 760-764.
- R. Liu, D. Wu, X. Feng and K. Müllen, *Angew. Chem. Int. Ed.* 2010, **122**, 2619-2623.
- S. Chen, J. Bi, Y. Zhao, L. Yang, C. Zhang, Y. Ma, Q. Wu, X. Wang and Z. Hu, *Adv. Mater.* 2012, **24**, 5593-5597.
- P. Chen, T.-Y. Xiao, Y.-H. Qian, S.-S. Li and S.-H. Yu, *Advanced Materials*, 2013, **25**, 3192-3196.
- J. Liang, X. Du, C. Gibson, X. W. Du and S. Z. Qiao, *Adv. Mater.* 2013, **25**, 6226-6231.
- Z. Jiang, Z.-j. Jiang, X. Tian and W. Chen, *J. Mater. Chem. A* 2014, **2**, 441-450.
- W. Wei, Y. Tao, W. Lv, F.-Y. Su, L. Ke, J. Li, D.-W. Wang, B. Li, F. Kang and Q.-H. Yang, *Sci. Rep.* 2014, **4**.
- J.-C. Li, P.-X. Hou, L. Zhang, C. Liu and H.-M. Cheng, *Nanoscale*, 2014, **6**, 12065-12070.
- R. Silva, D. Voiry, M. Chhowalla and T. Asefa, *J. Am. Chem. Soc.* 2013, **135**, 7823-7826.
- Y. Chang, F. Hong, C. He, Q. Zhang and J. Liu, *Adv. Mater.* 2013, **25**, 4794-4799.
- D. Yu, Q. Zhang and L. Dai, *J. Am. Chem. Soc.* 2010, **132**, 15127-15129.
- X.-K. Kong, C.-L. Chen and Q.-W. Chen, *Chem. Soc. Rev.* 2014, **43**, 2841-2857.
- J. Du, F. Cheng, S. Wang, T. Zhang and J. Chen, *Sci. Rep.* 2014, **4**.
- J. Liang, R. F. Zhou, X. M. Chen, Y. H. Tang and S. Z. Qiao, *Adv. Mater.* 2014, **26**, 6074-6079.
- H. Yin, C. Zhang, F. Liu and Y. Hou, *Adv. Funct. Mater.* 2014, **24**, 2930-2937.
- Y. Liang, Y. Li, H. Wang, J. Zhou, J. Wang, T. Regier and H. Dai, *Nat. Mater.* 2011, **10**, 780-786.
- T. Wang, J. Tang, X. Fan, J. Zhou, H. Xue, H. Guo and J. He, *Nanoscale*, 2014, **6**, 5359-5371.
- J. Tang, T. Wang, X. Pan, X. Sun, X. Fan, Y. Guo, H. Xue and J. He, *J. Phys. Chem. C* 2013, **117**, 16896-16906.
- R. Jasinski, *Nature*, 1964, **201**, 1212-1213.
- D. Huang, Y. Luo, S. Li, B. Zhang, Y. Shen and M. Wang, *Nano Res.* 2014, **7**, 1054-1064.
- X.-J. Huang, Y.-G. Tang, L.-F. Yang, P. Chen, Q.-S. Wu and Z. Pan, *J. Mater. Chem. A* 2015, **3**, 2978-2984.
- J. Zhang, D. He, H. Su, X. Chen, M. Pan and S. Mu, *J. Mater. Chem. A* 2014, **2**, 1242-1246.
- Z. Xiang, Y. Xue, D. Cao, L. Huang, J.-F. Chen and L. Dai, *Angew. Chem. Int. Ed.* 2014, **53**, 2433-2437.
- D. Zhao, J.-L. Shui, L. R. Grabstanowicz, C. Chen, S. M. Commet, T. Xu, J. Lu and D.-J. Liu, *Adv. Mater.* 2014, **26**, 1093-1097.
- W. Niu, L. Li, X. Liu, N. Wang, J. Liu, W. Zhou, Z. Tang and S. Chen, *J. Am. Chem. Soc.* 2015, **137**, 5555-5562.
- W. Xia, R. Zou, L. An, D. Xia and S. Guo, *Energy Environ. Sci.* 2015, **8**, 568-576.
- G. Yang, W. Choi, P. Xiong and C. Yu, *Energy Environ. Sci.* 2015, **8**, 1799-1807.
- F. Jaouen, E. Proietti, M. Lefevre, R. Chenitz, J.-P. Dodelet, G. Wu, H. T. Chung, C. M. Johnston and P. Zelenay, *Energy Environ. Sci.* 2011, **4**, 114-130.
- Z. Chen, D. Higgins, A. Yu, L. Zhang and J. Zhang, *Energy Environ. Sci.* 2011, **4**, 3167-3192.
- D.-W. Wang and D. Su, *Energy Environ. Sci.* 2014, **7**, 576-591.
- E. Proietti, F. Jaouen, M. Lefèvre, N. Larouche, J. Tian, J. Herranz and J.-P. Dodelet, *Nat. Commun.* 2011, **2**, 416.
- D.-S. Yang, S. Chaudhari, K. P. Rajesh and J.-S. Yu, *ChemCatChem*, 2014, **6**, 1236-1244.
- F. J. Pérez-Alonso, M. A. Salam, T. Herranz, J. L. Gómez de la Fuente, S. A. Al-Thabaiti, S. N. Basahel, M. A. Peña, J. L. G. Fierro and S. Rojas, *J. Power Sources* 2013, **240**, 494-502.
- Z. Yang, X. Zhou, Z. Jin, Z. Liu, H. Nie, X. a. Chen and S. Huang, *Adv. Mater.* 2014, **26**, 3156-3161.
- R. Cao, R. Thapa, H. Kim, X. Xu, M. Gyu Kim, Q. Li, N. Park, M. Liu and J. Cho, *Nat. Commun.* 2013, **4**.
- S. Kundu, T. C. Nagaiah, W. Xia, Y. Wang, S. V. Dommele, J. H. Bitter, M. Santa, G. Grundmeier, M. Bron, W. Schuhmann and M. Muhler, *J. Phys. Chem. C* 2009, **113**, 14302-14310.
- Z. Chen, D. Higgins, H. Tao, R. S. Hsu and Z. Chen, *J. Phys. Chem. C* 2009, **113**, 21008-21013.
- Y. Yao, H. Xiao, P. Wang, P. Su, Z. Shao and Q. Yang, *J. Mater. Chem. A* 2014, **2**, 11768-11775.
- H. T. Chung, J. H. Won and P. Zelenay, *Nat. Commun.* 2013, **4**, 1922.
- W. Yang, X. Liu, X. Yue, J. Jia and S. Guo, *J. Am. Chem. Soc.* 2015, **137**, 1436-1439.
- C. Wang, M. Waje, X. Wang, J. M. Tang, R. C. Haddon and Yan, *Nano Lett.*, 2004, **4**, 345-348.
- G. Wu, K. L. More, P. Xu, H.-L. Wang, M. Ferrandon, A. J. Kropf, D. J. Myers, S. Ma, C. M. Johnston and P. Zelenay, *Chem. Commun.*, 2013, **49**, 3291-3293.
- Y. Zhang, J. Ge, L. Wang, D. Wang, F. Ding, X. Tao and W. Chen, *Sci. Rep.* 2013, **3**.

ARTICLE

Journal Name

50. D. Shin, B. Jeong, B. S. Mun, H. Jeon, H.-J. Shin, J. Baik and J. Lee, *J. Phys. Chem. C* 2013, **117**, 11619-11624.
51. C. V. Rao, C. R. Cabrera and Y. Ishikawa, *J. Phys. Chem. Lett.* 2010, **1**, 2622-2627.
52. Z. Mo, S. Liao, Y. Zheng and Z. Fu, *Carbon*, 2012, **50**, 2620-2627.
53. A. Dorjgotov, J. Ok, Y. Jeon, S.-H. Yoon and Y. Shul, *J. Appl. Electrochem.* 2013, **43**, 387-397.
54. L. Lin, Q. Zhu and A.-W. Xu, *J. Am. Chem. Soc.* 2014, **136**, 11027-11033.
55. J. D. Wiggins-Camacho and K. J. Stevenson, *The J. Phys. Chem. C* 2011, **115**, 20002-20010.
56. G. Ma, R. Jia, J. Zhao, Z. Wang, C. Song, S. Jia and Z. Zhu, *J. Phys. Chem. C* 2011, **115**, 25148-25154.
57. Y. Li, W. Zhou, H. Wang, L. Xie, Y. Liang, F. Wei, J.-C. Idrobo, S. J. Pennycook and H. Dai, *Nat. Nanotechnol.*, 2012, **7**, 394-400.
58. H.-P. Cong, P. Wang, M. Gong and S.-H. Yu, *Nano Energy*, 2014, **3**, 55-63.
59. T.-N. Ye, L.-B. Lv, X.-H. Li, M. Xu and J.-S. Chen, *Angew. Chem. Int. Ed.*, 2014, **53**, 6905-6909.
60. S. Lee, M. Choun, Y. Ye, J. Lee, Y. Mun, E. Kang, J. Hwang, Y.-H. Lee, C.-H. Shin, S.-H. Moon, S.-K. Kim, E. Lee and J. Lee, *Angew. Chem. Int. Ed.*, 2015, **54**, 9230-9234.
61. J. Zhang, Z. Zhao, Z. Xia and L. Dai, *Nat. Nanotechnol.*, 2015, **10**, 444-452.
62. Y.-P. Zhu, Y. Liu, Y. Liu, T. Ren, G. Du, T. Chen and Z.-Y. Yuan, *J. Mater. Chem. A*, 2015, **3**, 11725-11729.
63. Y. Hou, Z. Wen, S. Cui, S. Ci, S. Mao and J. Chen, *Adv. Funct. Mater.* 2015, **25**, 871-871.